Very-high-order harmonic generation from Ar atoms and Ar^+ ions in superintense pulsed laser fields: An *ab initio* self-interaction-free time-dependent density-functional approach

Juan J. Carrera,[1] Shih-I Chu,[1,*] and X. M. Tong[2]

[1]*Department of Chemistry, University of Kansas, and Kansas Center for Advanced Scientific Computing, Lawrence, Kansas 66045, USA*

[2]*J. R. Macdonald Laboratory, Physics Department, Kansas State University, Manhattan, Kansas 66506, USA*

(Received 14 January 2005; published 21 June 2005)

We present an *ab initio* nonpertubative investigation of the mechanisms responsible for the production of very-high-order harmonic generation (HHG) from Ar atoms and Ar^+ ions by means of the self-interaction-free time-dependent density-functional theory recently developed. Further, by introducing an effective charge concept, we can study at which laser intensity the contribution to the high-energy HHG from Ar^+ ions precede over the Ar atoms. Comparing the HHG behavior from Ar atoms and Ar^+ ions in the superintense laser field, we conclude that the high-energy HHG observed in the recent experiment originated from the ionized Ar atoms.

DOI: 10.1103/PhysRevA.71.063813 PACS number(s): 42.65.Ky, 32.80.Wr, 71.15.Mb

Multiple high-order harmonic generation (HHG) is one of the most rapidly developing topics in the field of laser-atom (molecule) interactions. When an intense laser field pulse is focused normally into an array of gas composed of either atoms or molecules, a highly nonlinear optical process can take place, producing a unique source of coherent light in the extreme ultraviolet (xuv) and soft x-ray regions of the spectra [1–3]. This coherent light is known as high-order harmonics. The physical origin of the HHG from linearly polarized (LP) laser field can be qualitatively understood by means of the rescattering model [4]: (1) the electron tunnels out the potential barrier when the laser field reaches the peak; (2) the tunneled electron is bounced back to the parent ionic core at a later time when the laser field changes to the opposite direction; (3) the returning electron emits a photon by the radiative recombination process. Based on this simple model, the highest photon energy (cutoff) is $I_p+3.2U_p$, where I_p is the ionization potential of the working material, $U_p=I/(4\omega^2)$ is the ponderomotive or quiver energy of electron in an oscillating electric field, I is the laser peak intensity, and ω is the laser frequency. Due to the ionization depletion, the HHG cutoff position in a superintense laser field is dependent upon the saturation intensity when the saturation intensity is lower than the laser peak intensity. The ionization depletion will limit the highest HHG one can obtain. The shortest wavelength generated by the HHG processes demonstrated today is taken place from He atoms and close to 500 eV [5,6], achieved by using ultrafast pulses (26 fs pulse duration) from a Ti:sapphire laser centered at 800 nm. He atom has the highest saturation intensity among all the neutral rare-gas atoms. However, the HHG yield from He atoms is several orders of magnitude lower than from other rare-gas atoms [7].

Comparing with the neutral Ar atom, the saturation intensity for each successive stage of ionization is progressively higher. This can in principle lead to considerable extension of the HHG cutoff energy. However, the emission intensity from the ions was found to be several orders of magnitude weaker than that from the neutral atoms [8]. Thus it was difficult to realize the generation of very-high-order harmonics from the ions in the past. However, a recent experiment [9] has achieved the realization of this process by using a waveguide geometry to limit plasma-induced laser beam defocusing and demonstrated the generation of very high-order harmonics from the Ar gas, up to 250 eV. The authors attributed the higher-energy photon to be the emission from the *ionized* Ar atoms. The experimental results are in qualitative agreement with the prediction from the Ammosov-Delone-Krainov (ADK) model [10]. However, the ADK model does not take into account the effect of detailed electron structure and ac Stark shift, etc., on the strong-field electron dynamics. Thus a more accurate theoretical formalism is required and desirable for quantitative exploration of this highly interesting multiphoton phenomenon.

To investigate the detailed mechanisms responsible for the production of the high-energy HHG, we perform an *ab initio* and systematic study of the HHG from Ar and Ar^+ in intense laser fields by means of the self-interaction-correction (or self-interaction-free) time-dependent density-functional theory (SIC-TDDFT) recently developed [7,11]. By comparing the HHG from Ar and Ar^+ as well as the survival probabilities of Ar and Ar^+ in the superintense laser field, we establish that the high-energy photon comes from the Ar^+ ions. Our predicted HHG cutoff positions are in good agreement with the recent experimental data [9]. Furthermore, we demonstrate that in a single calculation, the SIC-TDDFT approach can be used to describe the creation of Ar^+ ions from Ag atoms and the HHG from Ar^+ ions dynamically.

The central equations of the SIC-TDDFT approach, for the nonperturbative treatment of multiphoton processes of many-electron atomic systems in an intense laser field, can be expressed as (in atomic units)

*Corresponding author: Electronic address: sichu@ku.edu

$$i\frac{\partial}{\partial t}\psi_{i\sigma}(\mathbf{r},t) = \hat{H}(\mathbf{r},t)\psi_{i\sigma}(\mathbf{r},t) = \left[-\frac{1}{2}\nabla^2 + V_{SIC,\sigma}^{OEP}(\mathbf{r},t)\right]\psi_{i\sigma}(\mathbf{r},t), \tag{1}$$

where $V_{SIC,\sigma}^{OEP}(\mathbf{r},t)$ is the time-dependent (TD) optimized effective potential (OEP) with SIC [7,11]. The TD-OEP–SIC equations can be solved for the individual time-dependent spin-orbital wave function in a self-consistent manner. Moreover, the single-particle time-dependent OEP-SIC is local (for every time step) and has the correct long-range $(-1/r)$ Coulombic potential behavior. The time evolution of the spin-orbital wave functions can be calculated by means of the time-dependent generalized pseudospectral (TDGPS) method [12]. The TDGPS method consists of the following two essential steps: (a) the spatial coordinates are optimally discretized in a *nonuniform* spatial grid by means of the generalized pseudospectral technique [13] with the use of only a modest number of grid points. This mesh is characterized by denser grids near the origin and sparser grids for large distances. (b) A second-order split-operator technique in the *energy* representation which allows the explicit elimination of undesirable fast-oscillating high-energy components is used for the time propagation of the wave function. The TDGPS technique has been shown to be both computationally considerably more efficient and accurate than the conventional time-dependent techniques using equal-spacing grid discretization. Detailed procedure for the construction of $V_{SIC,\sigma}^{OEP}(\mathbf{r},t)$ and the solution of the above TD-OEP–SIC equations can be found in our recent works [7,11].

Once the individual time-dependent spin-orbital wave functions $\{\psi_{i\sigma}(\mathbf{r},t)\}$ are obtained, we can determine the time-dependent induced dipole moment as

$$d(t) = \int z\rho(\mathbf{r},t)d\mathbf{r} = \sum_{i\sigma} d_{i\sigma}(t),$$

where

$$d_{i\sigma}(t) = n_{i\sigma}\langle\psi_{i\sigma}(\mathbf{r},t)|z|\psi_{i\sigma}(\mathbf{r},t)\rangle$$

is the induced dipole moment of the ith spin orbital and $n_{i\sigma}$ is its electron occupation number. The power spectrum of the HHG is then acquired by taking the Fourier transform of the total time-dependent induced dipole moment $d(t)$:

$$P(\omega) = \left|\frac{1}{t_f - t_i}\int_{t_i}^{t_f} d(t)e^{-i\omega t}dt\right|^2. \tag{2}$$

To facilitate the detailed analysis of the relative contribution of Ar and Ar^+ to HHG, we introduce a time-dependent effective charge (TDEC) as

$$Z_{eff}(t) = Z - \sum_{i\sigma} n_{i\sigma}\int |\psi_{i\sigma}(\mathbf{r},t)|^2 d\mathbf{r}, \tag{3}$$

which characterizes the dynamic ionization processes. The partial time-dependent ionization probabilities of Ar atom and Ar^+ ion are computed from its individual valence electron orbital ($3s$, $3p_{\pm 1}$, and $3p_0$). It is imperative to mention that all the valence electrons are treated explicitly and each contributes to the total effective potential and multiphoton processes.

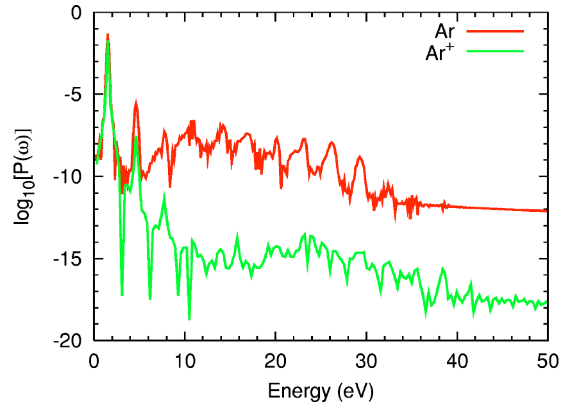

FIG. 1. (Color online) The HHG spectra of Ar atoms (thin line) and Ar^+ ions (thick line) in a laser field with $\sin^2$ pulse shape, peak intensity $I=5.0\times 10^{13}$ W/cm^2, and wavelength $\lambda=800$ nm.

Based on the SIC-TDDFT method, we shall investigate the HHG process from the Ar atoms (and the Ar^+ ions) in linearly polarized intense laser fields. An 18-fs laser pulse duration with $\sin^2$ pulse shape was used throughout the calculations. In the time propagation, the radial grid extends up to a minimum of 100 a.u. which is almost twice the maximum quiver radius $R=2\sqrt{I}/\omega^2$. To avoid unphysical reflections and oscillations of the wave function due to the finite radius size in the simulation, an absorber [12] is specifically placed at 60 a.u. Furthermore, up to 1000 radial grid points (for each partial wave) and 70 partial waves were used to ensure full convergence of the time-dependent wave functions and HHG power spectra.

In a weak laser field, the HHG's from Ar atoms and Ar^+ ions are significantly different as presented in Fig. 1. The cutoff position of HHG from Ar^+ ions is higher than that from Ar atoms, but the HHG yield from Ar^+ is significantly lower (by several orders of magnitude) than that of Ar. This indicates that the smaller the ionization potential (e.g., I_p for Ar^+ is 27.6 eV and for Ar is 15.8 eV), the larger the HHG yield, but the shorter the harmonic cutoff frequency. On the other hand, the effective charges are close to 0 for Ar and 1 for Ar^+, which means that the ionization is negligible in a relatively weak field and the HHG's from Ar and Ar^+ can be well differentiated. In stronger laser peak intensities but below the saturation intensity of Ar, the latter occurs at about 7.7×10^{14} W/cm^2 and substantial ionization of the atom is observed. As we move to the superstrong laser field intensity regime (such as 1.3×10^{15} W/cm^2), the high-energy HHG's (>180 eV) from Ar and Ar^+ are close to each other as shown in Fig. 2(a). To show more clearly the HHG from the Ar^+ ions and Ar atoms near the cut off regime, we plot them in Fig. 2(b). In the lower-energy part (<180 eV), the HHG from Ar atoms are higher than that from Ar^+ ions. The results shown in Fig. 2(a) can be understood as follow. The Ar atoms are first ionized to Ar^+. During the ionization process, they can also emit the lower-energy HHG. The ionized Ar atoms can survive in a superintense laser field and emit the higher-energy HHG as well as the lower-energy HHG, but

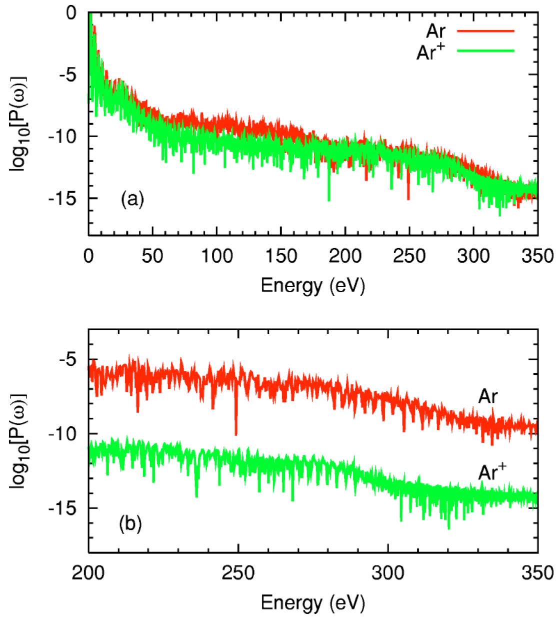

FIG. 2. (Color online) (a) The HHG spectra of Ar atoms and Ar^+ ions in a laser field with $\sin^2$ pulse shape, peak intensity $I=1.3\times10^{15}$ W/cm^2, and wavelength $\lambda=800$ nm. (b) The HHG power spectra of Ar^+ and Ar near the cutoff regime. For better visualization, we upshift the Ar HHG spectra by five orders.

the HHG yield is lower than that from neutral Ar atoms. In the high-energy regime, the calculated HHG from Ar and Ar^+ are closer to each other, but not identical. This is due to the fact that HHG's directly from Ar^+ ions and HHG from ionized Ar are different. The HHG from Ar^+ starts from the Ar^+ ground state; one electron from the neutral atom is already gone to start with. The HHG from the ionized Ar starts from the Ar ground state, and the ionized electron is still around the parent ionic core. The calculated cutoff position around 280 eV (both from Ar and Ar^+ curves) as shown in Fig. 2(b) is in reasonable agreement with the experimental data (250 eV) [9]. The experimental cutoff is probably lowered by the propagation effects which we ignored in the present simulation. This clearly shows that the extended HHG is due to the contribution from the ionized Ar atoms. The HHG spectra from the higher intensity (Fig. 2) are almost continuous instead of individual HHG peaks observed in the lower laser intensity (Fig. 1).

In addition, the Ar atom's power spectrum features important and salient characteristics. First, a second plateau becomes clearly discerned about 180 eV. The harmonic yield for the second plateau is at least two orders of magnitude (in logarithmic scale) smaller than the first plateau. The nature of the second plateau can be well correlated to the notion that the contribution to the high-frequency harmonics is evidently not due to Ar but rather to Ar^+. As a result, the harmonics produced by both systems, again at the high-frequency regime, mimic each other rather well. Therefore, the extension of the cutoff in laser intensities above the saturation intensity is explicitly due to the argon ions as it was well observed in the experiment. Hence, the importance of the TDDFT calculations is paramount in this calculation since a single-active-electron model would fail for the present case due to the

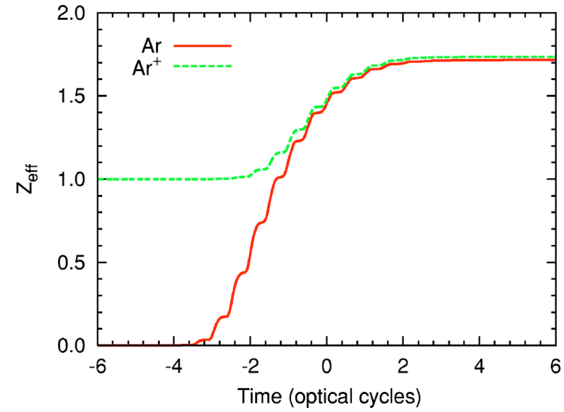

FIG. 3. (Color online) The time-dependent effective charge for Ar and Ar^+ in the laser field with $\sin^2$ pulse shape, peak intensity $I=1.3\times10^{15}$ W/cm^2, and wavelength $\lambda=800$ nm.

strong if not almost complete ionization of Ar.

Figure 3 shows the time-dependent effective charge of Ar and Ar^+ in the supperintense laser fields. The laser peak field used is 1.3×10^{15} W/cm^2 with center wavelength $\lambda=800$ nm. Clearly we discern that the effective charge for Ar^+ increases slowly from 1 to about 1.7 when the field is over. The effective charge of Ar atoms increases dramatically from three optical cycles before the peak laser intensity and approaches the Ar^+ effective charge around one optical cycle before the peak laser intensity is reached. This means that the Ar is ionized to Ar^+ within two optical cycles. Then, the effective charge of Ar follows the effective charge of Ar^+ in the later time. The effective charge of both the Ar atom and Ar^+ ion at the end of the pulse is very similar, indicating that the final states of both systems are similar. Therefore, we can conclude that the HHG in the high-energy regime is from the ionized Ar atoms, which is consistent with our conclusion from comparison of the HHG from Ar and Ar^+. We also have studied the HHG from Ar and Ar^+ at peak laser intensity 9×10^{14} W/cm^2. The predicted cutoff position (130 eV) is also in good agreement with the recent experiment at the same peak intensity [9]. Note that the difference of HHG in

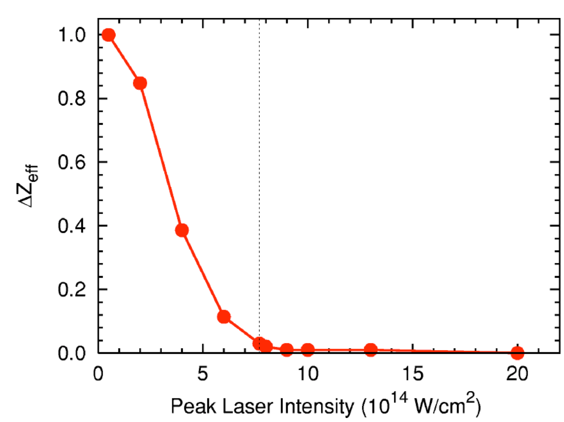

FIG. 4. (Color online) The difference of the effective charge for Ar and Ar^+ as a function of peak laser intensity when the field is over. The dotted vertical line marks the saturation intensity of Ar ($=7.7\times10^{14}$ W/cm^2).

the high-energy regime from Ar atoms and Ar^+ ions is larger than that at higher laser intensities. The difference of the effective charge for Ar atoms and Ar^+ ions when the field is over is also larger than that at a higher intensity. This implies that the contribution from the ionized Ar atom decreases as the laser intensity decreases.

To further explore the contribution from the ionized Ar, we plot in Fig. 4 the difference of the effective charge of Ar^+ ions and Ar atoms at the end of the laser pulse as a function of the laser intensity. The difference of the effective charges decreases as the laser intensity increases. Before it reaches the saturation intensity, the HHG mainly comes from the neutral atoms. When the laser intensity is stronger than the saturation intensity, the HHG is mainly contributed from the ionized Ar. Figures 1 and 2 show the behavior of these two limits (weak- and superintense-field cases).

Based on the SIC-TDDFT formalism, we have studied the mechanism of HHG from ionized Ar atoms. The HHG in the high-energy regime mainly comes from the ionized Ar atoms when the laser intensity is higher than the saturation intensity. On the other hand, the HHG is contributed mainly from the neutral atoms when the laser intensity is lower than the saturation intensity. All these findings and the predicted cutoff positions are in good agreement with the recent experiment [9]. Furthermore, our study shows that the SIC-TDDFT can provide a powerful nonpertubative approach for the description of the creation of the Ar^+ ions from Ar atoms and the generation of very high-order harmonics from Ar^+ ions within a single calculation. Of course, the present simulation presented the state-of-the-art calculation of the single-atom response. To compare with the experiment in detail, we have to consider the propagation effects and the volume effects.

This work was supported by the Chemical Sciences, Geosciences and Biosciences Division of the Office of Basic Energy Sciences, Office of Science, U.S. Department of Energy. We acknowledge the Kansas Center for Advanced Scientific Computing for the support of supercomputer time.

[1] J. J. Macklin, J. D. Kmetec, and C. L. Gordon III, Phys. Rev. Lett. **70**, 766 (1993).
[2] E. Seres, J. Seres, F. Krausz, and C. Spielmann, Phys. Rev. Lett. **92**, 163002 (2004).
[3] J. Zhou, J. Peatross, M. M. Murnane, H. C. Kapteyn, and I. P. Christov, Phys. Rev. Lett. **76**, 752 (1996).
[4] P. B. Corkum, Phys. Rev. Lett. **71**, 1994 (1993).
[5] C. Spielmann, N. H. Burnett, S. Sartania, R. Koppitsch, M. Schnurer, C. Kan, M. Lenzner, P. Wobrauschek, and F. Krausz, Science **278**, 661 (1997).
[6] Z. Chang, A. Rundquist, H. Wang, M. M. Murnane, and H. C. Kapteyn, Phys. Rev. Lett. **79**, 2967 (1997).
[7] X. M. Tong and Shih-I Chu, Phys. Rev. A **64**, 013417 (2001).
[8] C.-G. Wahlstrom, S. Borgstrom, J. Larsson, and S.-G. Pettersson, Phys. Rev. A **51**, 585 (1995).
[9] E. A. Gibson, A. Paul, N. Wagner, R. Tobey, S. Backus, I. P. Christov, M. M. Murnane, and H. C. Kapteyn, Phys. Rev. Lett. **92**, 033001 (2004).
[10] M. V. Ammsov, N. B. Delone, and V. P. Krainov, Sov. Phys. JETP **64**, 1191 (1964).
[11] X. M. Tong and Shih-I Chu, Phys. Rev. A **57**, 452 (1998).
[12] X. M. Tong and Shih-I Chu, Chem. Phys. **217**, 119 (1997).
[13] G. Yao and Shih-I Chu, Chem. Phys. Lett. **204**, 381 (1993).